Eur. Phys. J. D **32**, 289–297 (2005)
DOI: 10.1140/epjd/e2005-00015-y

THE EUROPEAN PHYSICAL JOURNAL D

Insights into positron annihilation lifetime spectroscopy by molecular dynamics simulations

Free-volume calculations for liquid and glassy glycerol

D. Račko[1,3], R. Chelli[2,3,a], G. Cardini[2,3], J. Bartoš[1], and S. Califano[2,3]

[1] Polymer Institute of SAS, 842 36 Bratislava, Slovak Republic
[2] Dipartimento di Chimica, Università di Firenze, Via della Lastruccia 3, 50019 Sesto Fiorentino, Italy
[3] European Laboratory for Non-linear Spectroscopy (LENS), Via Nello Carrara 1, 50019 Sesto Fiorentino, Italy

Received 10 August 2004 /Received in final form 17 November 2004
Published online 1st February 2005 –

Abstract. The relationship between free-volume properties measured from positron annihilation lifetime spectroscopy (PALS) and calculated from molecular dynamics simulations has been investigated for glassy and liquid glycerol in the temperature range 150–400 K. A virtual probing procedure has been developed to retrieve information on the basic free-volume properties of the simulated microstructures, i.e. mean cavity volume and free-volume cavity fractions. Our data leads us to infer on the occurrence of experimentally non-detectable small cavities with mean equivalent radius of 1.8–1.9 Å between 250 and 275 K. The size of these limiting cavities is found to be temperature dependent, being smaller at low temperatures. At high temperatures, above a characteristic PALS temperature T_{b2}^{L}, the formation of very large cavities is predicted. This finding suggests that, when the dimension of the holes in the system exceeds a given value, the PALS measurements become unable to catch the complete structural information and phenomena of dynamical origin enter into play in the PALS signal decay. The calculated number of cavities is found to be almost independent on the temperature from the glassy up to the liquid phase, thus furnishing a certain support to theoretical models proposed to evaluate the free-volume cavity fractions.

PACS. 61.20.Ja Computer simulation of liquid structure – 78.70.Bj Positron annihilation

1 Introduction

Positron annihilation lifetime spectroscopy (PALS), based on the annihilation process of positrons [1–3], has rapidly become an established method for structural and dynamical investigation of condensed matter. In most non-conducting materials, such as organic compounds, positron annihilation occurs through the formation of transiently bound electron-positron pairs, the so-called positronium (Ps). According to the mutual spin orientation of the pair partners, the occurrence of ortho-positronium (o-Ps) or para-positronium (p-Ps) can be detected in the annihilation signal, with appropriate relative intensities. In contrast to p-Ps, the o-Ps lifetimes are strongly temperature dependent. o-Ps bound states have long lifetimes, typically from 1 to 5 ns in condensed phases. They supply a very sensitive probe for the occurrence of local regions of reduced electron density in disordered materials. Lifetime measurements are actually used to compute the dimensions of the mean free-volume holes in condensed systems by application of a semi-empirical equation [4]. This relation, based on the quantum mechanical model of Tao [5], modified by Eldrup et al. [6] and by Nakanishi et al. [7] for the temperature dependence of discrete lifetimes, predicts that o-Ps lives for longer time in larger free-volume holes. This model, referred as the "standard model", assumes spherical-shaped holes and an infinitely deep potential well. Other models, differing in the form of the potential equation for o-Ps in matrix, have also been proposed to relate the o-Ps lifetime with the hole radius [8].

PALS is presently the only experimental method for the direct detection of the local free-volume at the atomic level. From PALS data one obtains both the mean free-volume hole size and the free-volume fraction. Available semi-empirical models for the calculation of the free-volume hole fraction from PALS data are based on Kovacs' approximations [9]. In general, the free-volume hole fraction is assumed to be proportional to the mean free-volume hole size and to the relative intensity of the o-Ps signal, where the latter is somehow related to the number density of holes [10–14]. In some systems, however, where the relative intensity does not change significantly, or for materials containing specific electron capturing groups, such as halogens, carbonyl etc. [15], the role of the relative intensity is neglected, implying a constant number of holes in the volume element [16,17]. In these models

[a] e-mail: chelli@chim.unifi.it

the so-called occupied volume is either kept constant [13] or allowed to vary with temperature [11,14,16,17]. The physical meaning of the occupied volume determined from PALS experiments is not yet clear, but it is assumed that it includes, in addition to the van der Waals contribution of the constituent particles, a free-volume term, inaccessible to the o-Ps probe, due to geometrical as well as to dynamical (vibrational or rotational motions) factors [3].

In the last decades there has been a large amount of work aimed to correlate the PALS data to different structural, dynamical and transport properties [13,14] in terms of the free-volume concept [18–22]. Despite the great progress in PALS methodology, the prediction of the total free-volume quantity remains indirect since it involves adjustable parameters. Instead Monte Carlo, molecular mechanics and molecular dynamics simulations allow us to obtain the free-volume quantities as non-adjustable parameters and here we shall show how these methods can be a useful complementary tool in free-volume studies.

The general "grid scanning" method is often used to compute the free-volume size and its distribution. The method includes the probing of simulated structures within constant [23,24] or variable [25,26] (e.g. random positions) grid spacing. In the case of constant grid spacing the free-volume is generally given as an integral of basic volume elements of constant value and geometry [24,27]. When the grid spacing decreases, the total free-volume approximates the solvent-excluded volume obtained from exact analytical methods proposed at first for the computation of solvent accessible areas for proteins [28–30]. In different methods the free-volume cavities are detected on the basis of the Delaunay triangulation [31] or Voronoi tessellation of space [24,32–35]. An improved algorithm for such a cavity construction and volume computation has been proposed [36].

In the literature only a few attempts to correlate the simulated free-volume with the free-volume hole from PALS experiments can be found. The free-volume fractions of low-molecular liquid above the glass transition temperature were calculated and compared with the PALS free-volume hole fractions [37]. Distributions of the free-volume cavity sizes in polymeric material were simulated employing an original computational method [26].

The aim of this research is to relate the probe accessible free-volume computed from molecular dynamics (MD) simulations [38,39] with the measured PALS free-volume in a wide temperature range and to discuss the origin of several PALS features. Glycerol has been chosen as a model system due to the fact that a complete set of MD simulations [40,41], PALS [42,43] data, and other relevant experimental data [44,45] is available.

The free-volume is obtained by virtual probing of the simulated microstructures. This approach allows us to handle the free-volume as a sum of discrete volume elements. In addition we predict the existence of a limit cavity volume below which the free-volume cavities are not detectable by PALS measurements. We also find that such a limit volume is temperature-dependent, being larger at higher temperatures. The formation of very large cavities above 300 K suggests that dynamical processes can be also involved in the PALS signal decay when the temperature of the system exceeds a characteristic PALS temperature T_{b2}^{L}. We also furnish a support to the hypothesis of temperature-independence of the number of cavities, on which several semi-empirical models [13,14,16,17] for the calculation of the free-volume cavity fraction are based.

The layout of the paper is as follows. The computational methods are described in Section 2. The free-volume properties are discussed and compared with experimental data in Section 3. The conclusions are given in Section 4.

2 Computational methods

2.1 Molecular dynamics simulations

Free-volume calculations were performed on configurations of liquid and glassy glycerol obtained by MD simulations. The potential model used, reported in reference [40], was adopted in previous MD simulation studies [40,41] to investigate micro-structural and dynamical properties related to the H-bond forming behavior of glycerol. The model was validated [40] by comparing several computed physical chemical properties with their experimental counterparts. Coulombic interactions were treated by the smooth particle mesh Ewald method [46], using a convergence parameter of 0.43 Å^{-1} and a grid spacing for the B-spline interpolation of charges of about 1 Å. Multiple (five) time step integration technique r-RESPA [47,48] was employed to integrate the equations of motion. Standard periodic boundary conditions were applied. Liquid and glassy samples of 300 molecules were obtained by cooling a sample equilibrated at 400 K and room pressure. The starting structure was obtained by distributing the molecular centers of mass at the nodes of a grid devised to regularly partition the cubic simulation box and by giving random orientations to the molecules. The structure was equilibrated under isobaric-isothermal thermodynamic conditions (NPT ensemble using the isotropic stress tensor constraint) at 400 K until the conformational distribution, the box side length and the potential energy fluctuated around constant values. The cooling run, from the initial temperature (400 K) down to 150 K, was made in steps of 10 K at a rate of 1.5×10^{12} K min^{-1} in the NPT thermodynamic ensemble. The chosen cooling rate is lower than that of previous MD simulations [40] (the effect of cooling rate and sample size on the glass transition has been discussed in Ref. [40]). The average box side length was then calculated from the last 100 ps of each NPT run and used for further constant volume constant energy (NVE ensemble) simulations. The NVE simulations were performed in two steps: a first run of 100 ps was used to equilibrate the system, then a production run of 200 ps followed. In order to prevent correlation between different configurations of the system, we recorded the atomic coordinates of subsequent system configurations at large distance in time (every 400 fs). All simulations were performed using the ORAC program [48].

2.2 Total free-volume and number of free-volume cavities

The main quantities obtained from PALS experiments are the mean hole volume and the free-volume hole fraction. In a simulation context, the former quantity corresponds to the ratio between the total free-volume of the cavities and their number [49], while the latter is the ratio between the total free-volume and the total volume of the simulation box. To evaluate these quantities, only two properties must be calculated: the total free-volume and the number of free-volume cavities, since the box volume is trivially obtained as output of the NPT simulations. The total free-volume in the simulated sample was obtained by numerical integration using a virtual probing with a o-Ps probe of radius [1–3] 0.53 Å. The atoms were modelled as hard spheres of appropriate van der Waals radii ($R_H = 1.2$ Å, $R_C = 1.7$ Å, $R_O = 1.52$ Å). In this approach the inserted probe tests the occurrence of a free space of a given geometry and selects an elementary volume element to measure the molecular and the free-volume space. In addition it furnishes the input for the free-volume calculation. In total, the free volume analysis has been performed on 13 000 structures (500 structures at each temperature). Free-volume data converged already after 100 ps (250 system configurations per simulation run), providing stable average values.

The probing procedure is as follows. The simulation box is partitioned into cubic grid elements, each of side length 0.5 Å. Then probe insertion trials are performed at all nodes of the grid. If at a given node the probe overlaps with an atom (periodic boundary conditions are considered in evaluating the overlap), the probe is not inserted. If in a cubic volume element there are n nodes occupied by inserted probes, the number n is assigned to that volume element. The free-volume is then evaluated according to the number associated to each volume element of the grid. Grid volume elements labelled with zero represent the probe inaccessible space in the simulated microstructures. Volume elements labelled with 1 contribute to the total free-volume by one eighth of the spherical probe volume (0.0779 Å^3). For the case of two probes sharing a volume element, the free-volume increment used is ∼0.1020 Å^3, for three is ∼0.1143 Å^3, for four is ∼0.1173 Å^3. If more than four probes occur in the same volume element, the element is considered in the inner (not a surface element) of a free-volume cavity. In this case the free-volume increment corresponding to the whole grid volume element (0.125 Å^3) is considered. These free-volume increments are obtained from additional geometric exploration and numerical integration. In this way the exact volume occupied by the inserted overlapping spherical probes represents the total free-volume in the simulated sample. Considerable time saving is achieved in this analytical approach for the calculation of the free-volume (3–6 seconds on a standard personal computer). The only drawback of the virtual probing method is that, due to the static grid and finite dimension of the probe, dense probe packing is not obtained. This problem is partially treated in the following, where the cavity building procedure is described.

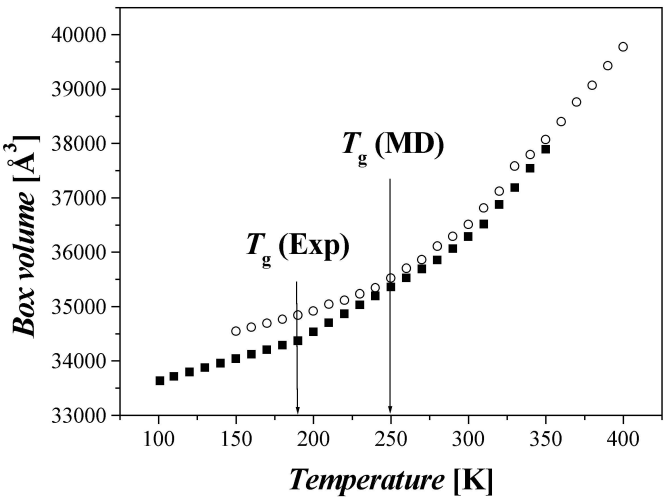

Fig. 1. Simulated (open circles) and experimental (filled squares) volume of 300 molecules of glycerol. Arrows mark experimental (from Ref. [50]) and simulated (from data of Fig. 3) glass transition temperature. Experimental data are taken from references [9,50].

The next quantity employed for the mean cavity volume calculation is the number of cavities in the simulation box. The cavities are determined on the basis of the geometrical analysis of overlaps between the inserted probes. A tolerance of one bit of the grid is applied for the overlap of probes. If the distance between two inserted probes is lower than two times the probe radius plus 0.5 Å, the two probes are considered to belong to the same cavity. For larger distances they are instead assumed to belong to different cavities. If two probes are found to belong to the same cavity using the tolerance criterion, then other probes are inserted at the nodes occurring in the space between them neglecting overlap with atoms. On the basis of the pairs of probes that are in contact, the map of the free-volume cavities is calculated. The number associated to each volume element is then updated on the basis of the new inserted probes and the definitive free-volume is calculated as explained before. The tolerance has been chosen on the basis of the comparison between the numbers of cavities obtained from the construction procedure working with grid spacing of 0.5 Å and with a grid spacing 10 times smaller (0.05 Å). Tolerance criteria were found to be active 100–150 times through the computation, depending on the temperature (less times at higher temperatures).

3 Results and discussion

3.1 Macroscopic volumes

The volume of the simulation box as a function of temperature is plotted in Figure 1 along with the volume occupied by 300 molecules (i.e. the number of molecules in the simulation box) calculated from experimental dilatometric

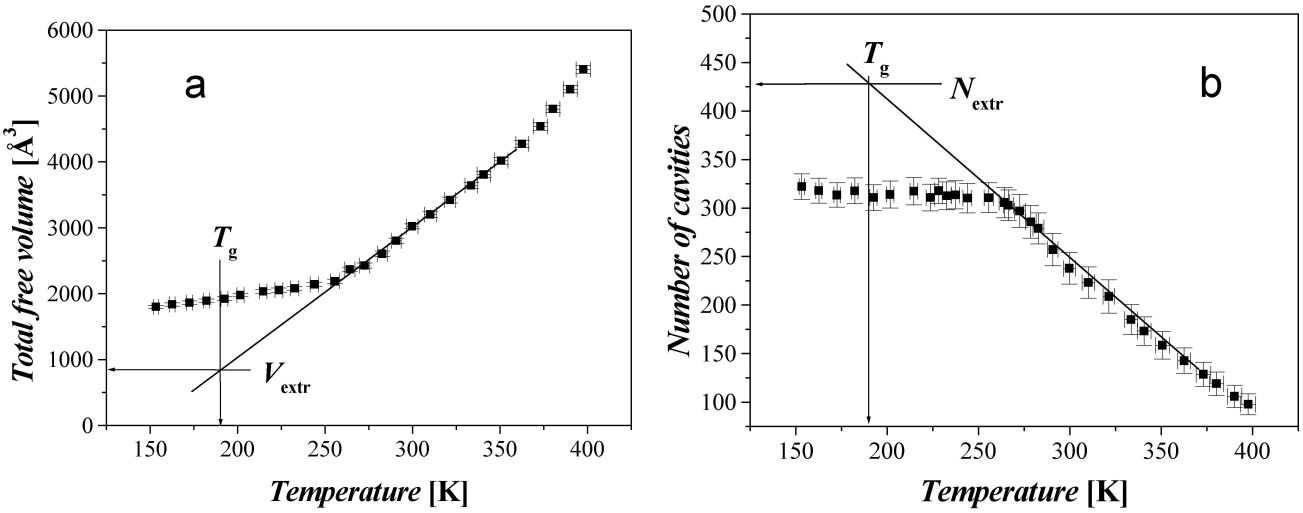

Fig. 2. (a) Total free-volume in the simulation box. $V_{\rm extr}$ is the total free-volume extrapolated to the experimental glass transition temperature ($T_{\rm g}$). (b) Number of cavities in the simulation box. $N_{\rm extr}$ is the number of cavities extrapolated to the experimental glass transition temperature.

data. This last quantity has been evaluated from the temperature dependence of the experimental density [9,50]. In the figure, the glass transition temperature determined from dilatometric measurements [50] ($T_{\rm g}$ = 190 K) and from the simulation is marked by arrows. The former temperature is in close agreement with the calorimetric [51] $T_{\rm g}$. Since the simulated $T_{\rm g}$ cannot be easily estimated from the box volume versus temperature curve, the $T_{\rm g}$ value reported in Figure 1 has been extracted from the trend of the mean cavity volume versus temperature reported and discussed in Section 3.3. This curve shows a well-evident bend at about 250 K, above an almost flat region typical of the glass state.

Both curves of Figure 1 show a change of curvature, characteristic of the glass transition [9]. The experimental and simulated volumes are in good agreement, the simulation slightly overestimating the volume by no more than 0.3% and 1.4% at higher and at lower temperatures, respectively. The larger disagreement in glass phase has been discussed in reference [40] as due to the faster cooling rate (of the order of a few nanoseconds at most) achieved in the simulation with respect to the typical experiment (of the order of minutes [9,50]). As a consequence the system is not at complete equilibrium and therefore a relaxed packing of the molecules is not achieved. Above 300 K a further slight change of slope occurs for both curves. The similarity of the curve slopes both in the glass and in the liquid indicates that the expansivity is well reproduced by the calculation.

3.2 Total free-volume and number of free-volume cavities

The total free-volume is plotted as a function of temperature in the range 150–400 K in Figure 2a. The temperature standard deviation ranges from 1.5 to 4.0 K from low to high temperatures, proving a good stability of the results as well as a reasonable thermal equilibration of the samples. The temperature dependence of the total free-volume is similar to that observed for the simulation box volume shown in Figure 1. Two linear regions with different slopes are well distinguished, with a discontinuity point at about 250 K. This shows that the technique of virtual o-Ps probing detects the glass transition in the simulated sample better than the density (see Fig. 1). In the glass the calculated free-volume is larger than in the real structure. This is again attributed to the fast cooling rate achieved in the simulations that does not allow the sample to be completely relaxed below the MD glass transition temperature.

The number of free-volume cavities in the simulated sample is shown as a function of temperature in Figure 2b. The decrease of the number of cavities with increasing temperature is due to the larger portions of local free-volume surrounding the molecules at higher temperature which increases the cavity aggregation. In the glass, the number of cavities is almost constant with temperature and thus only a slight slope of the curve is observed. This slope has the same origin as in the liquid, its moderate entity being due to the fact that only small structural rearrangements of the molecules can occur in the glass.

Since at higher temperatures the liquid system is closer to ergodicity than below the glass transition, a more realistic estimate of the free-volume at the glass transition temperature can be obtained assuming that the linear trend of the free-volume temperature dependence observed in the liquid would persist down to the experimental glass transition temperature under ergodic conditions. Hence, by extrapolation of the curve, as shown in Figure 2a, we obtain a total free-volume of $\sim$900 Å^3 for the glass, which is almost one half of that computed at the simulated glass transition point. In the same way we can better estimate

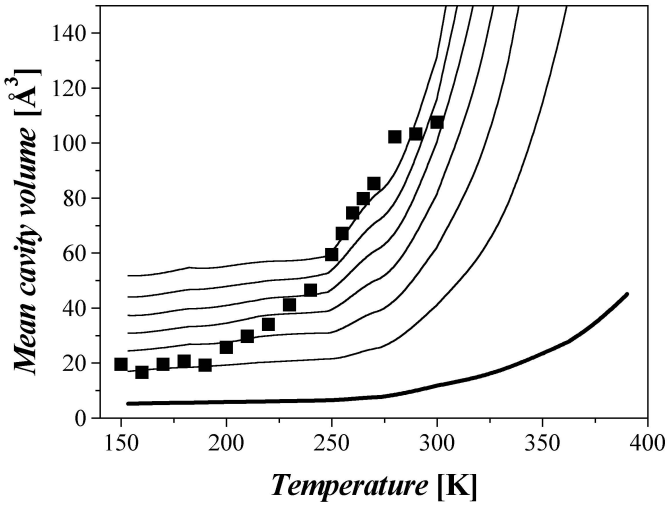

Fig. 3. Mean hole volumes from PALS measurements [42,43] (filled squares) and mean cavity volumes from MD simulations (bold line) as a function of temperature. Thin lines refer to mean cavity volumes calculated excluding cavities with a volume smaller than a given threshold $V_{\rm lim}$ (from bottom to top $V_{\rm lim}$ = 5, 10, 15, 20, 25 and 30 Å^3).

the number of cavities at the experimental glass transition temperature (see Fig. 2b) obtaining a value of 430 cavities versus 320 cavities computed at the simulated transition temperature. However the change of slope of the number of cavities at about the simulated glass transition temperature observed in Figure 2b can be also interpreted without calling into play the transition from glass to liquid, or vice versa. This will be discussed in Section 3.4 where we show that, by exclusion of very small cavities from the calculation, the number of cavities remains constant until about 300 K.

3.3 Mean cavity volume

The mean cavity volumes calculated for the static configurations from MD simulations are plotted as a function of temperature in Figure 3 together with the experimental PALS mean hole volumes [42,43]. In the glass both the PALS and the calculated mean cavity volumes are almost constant, the latter being roughly one fourth of the former. The calculated mean cavity volumes differ even more from the experimental ones in the liquid, being about 10 times smaller at room temperature. While the experimental PALS mean hole volumes are strongly temperature dependent, the calculated mean cavity volumes show only a slight dependence with temperature. On the basis of the good agreement found between calculated and experimental volumes (see Fig. 1), it is difficult to explain the large discrepancies occurring between calculations and experiments for the mean cavity volumes. In order to prove that the disagreement between calculation and experiment is not due to the radius of the probe adopted in the virtual probing procedure, additional calculations were performed using different probe radius. In the PALS literature [1–3]

Table 1. Number of cavities $N_{\rm C}$, total free-volume $V_{\rm f}$ (in Å^3) and mean cavity volume $\overline{V}_C$ (in Å^3) calculated for glass (150 K) and for liquid (300 K) glycerol using different probe radii, $R_{\rm p}$ (in Å).

	Glass			Liquid		
$R_{\rm p}$	$N_{\rm C}$	$V_{\rm f}$	$\overline{V}_C$	$N_{\rm C}$	$V_{\rm f}$	$\overline{V}_C$
0.53	321.9	1672.3	5.2	237.7	2804.1	11.8
0.6	262.2	1475.2	5.6	254.7	2461.3	9.7
1.2	0.0	0.0	0.0	10.0	72.3	7.2

different values of the o-Ps radius have been used, ranging from a minimum of 0.53 Å, obtained from the quantum-mechanical description of o-Ps [1,2], to a maximum of 1.2 Å, corresponding to the van der Waals radius of the hydrogen atom. In Table 1, we summarize the results obtained with three different probe radii (0.53, 0.6 and 1.2 Å) in the glass at 150 K and in the liquid at 300 K. In the glass the probe of radius 0.6 Å lowers the total free-volume by about 200 Å^3 and the number of cavities by 60, with respect to the original probe of 0.53 Å. This means that small cavities, still detectable with the 0.53 Å probe radius, are not detected anymore by increasing the probe radius, and therefore the mean cavity volume slightly increases. In the liquid the increase of the probe radius from 0.53 Å to 0.60 Å has the opposite effect, since it enhances the number of cavities and decreases the mean cavity volume. In the liquid there is in fact only a limited fraction of small cavities and therefore an increase of the probe radius has the main effect to break larger cavities, thus increasing their number and reducing the mean cavity volume. For a radius of 1.2 Å, no probe can be inserted into the glassy sample. In the liquid the total free-volume drops of almost two orders of magnitude, since in this case the effect of cavity breaking is so large that the free-volume of 72.3 Å^3 originates only from 10 cavities each of volume 7.2 Å^3 (the probe volume). The small variations in the mean cavity volume observed as a function of the probe radius, far from being able to fit the experimental data of Figure 3, show that the difference between calculation and experiment cannot be due to the probe size used in the probing procedure. We have therefore considered the possibility that it could originate from an intrinsic feature of the PALS experiments. Past theoretical studies, adopting a finite spherical potential well model [54] have actually suggested the existence of a lower limit for the volume of the cavities detectable by o-Ps in a PALS experiment. In order to verify the validity of this hypothesis and to estimate the volume of these limiting cavities, we have calculated the mean cavity volume excluding cavities of volume smaller than a threshold value, $V_{\rm lim}$. The mean cavity volumes obtained for different values of $V_{\rm lim}$ are plotted in Figure 3 as a function of temperature. The curves calculated for the chosen $V_{\rm lim}$ values all share the same temperature dependence, remarkably similar to that of the experimental mean hole volume. We consider this as a strong argument in favor of the existence of smallest detectable cavities.

In the low temperature limit a good agreement with the experimental data is obtained using for $V_{\rm lim}$ a value of 5 Å^3. At higher temperatures, i.e. at temperatures for which the MD simulations give more reliable results, good agreement is found for larger values of $V_{\rm lim}$. For example, in the temperature range 250–275 K the best agreement is obtained using $V_{\rm lim}$ equal to 25–30 Å^3. The radius of the equivalent spherical cavity is 1.8–1.9 Å, in good agreement with the value [54] of 1.85 Å, obtained with a theoretical model used to interpret PALS experiments for copolymers of organic acids [52] and polystyrenes [26]. The value of $V_{\rm lim}$ characterizes a portion of the total number of free-volume sites that are eliminated for o-Ps localization due to some mobility on a short time scale (below a few nanoseconds) as suggested in a recent PALS study [43].

In order to explain the temperature dependence of $V_{\rm lim}$ we recall that the method adopted in this work to compute the free-volume is static in nature, implying the evaluation of the free-volume on "uncorrelated configurations". As pointed out before, this procedure, albeit fast, has the drawback of ignoring the thermal motion of the atoms. It has been suggested that in PALS experiments only cavity volumes with sufficiently long lifetime can be detected. The limiting cavity volume detected by PALS experiments must be therefore necessarily temperature dependent, since very small cavities, at the limit of detection at low temperatures, will be reduced in size at higher temperatures due to the larger thermal motions of the atoms and became further non-detectable. This conclusion is fully consistent with the data of Figure 3. While the mean cavity volume is of the order of 60–100 Å^3 in the liquid above 250 K, corresponding to a value of $V_{\rm lim}$ of the order of 25–30 Å^3, at the temperatures of the glass the mean cavity volume is reduced to 20 Å^3, corresponding to a $V_{\rm lim}$ of about 5 Å^3.

An additional feature of the experimental mean hole volume of Figure 3 is the presence of a curvature break in the high temperature region giving rise to a second characteristic temperature T_{b2}^L occurring at 290 K. Recent correlations between the PALS data and the relevant dynamic properties of glycerol and polybutadiene [42], suggest that the most suitable candidate for the break at T_{b2}^L is the primary α-relaxation. Our analysis of the data is not able to catch this phenomenon, due to the static nature of the proposed method of analysis. Since the mean cavity volume is the ratio between the total free-volume and the number of cavities, the break at T_{b2}^L can arise either from a decrease of the total free-volume or from an increase of the number of cavities. As shown in Figure 2b, the number of cavities decreases with increasing temperature, and thus the latter case can be excluded. In the former case, the total free-volume may decrease because some cavities could become too large at higher temperature for detection by PALS. The upper limit of validity of the quantum-mechanical model of o-Ps used to determine the equivalent spherical hole size has been found [2,7] to be $R_{\rm h} \sim 10$ Å. Such large cavities are not present in the investigated simulated samples until about 380 K. However, starting at about 290 K, our simulations give rise

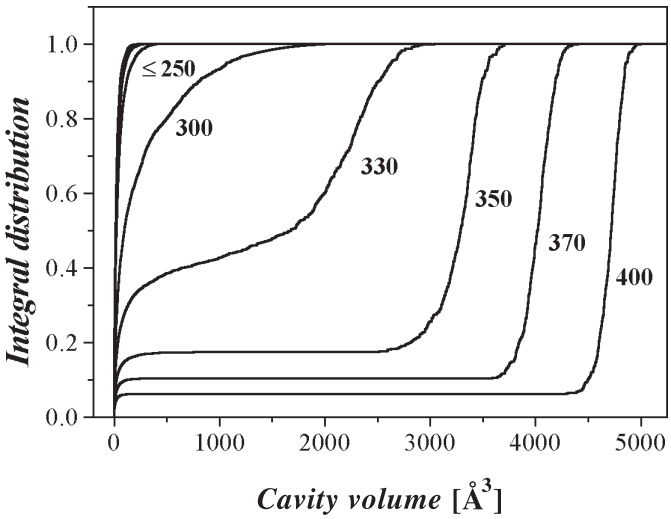

Fig. 4. Integral distribution of the ratio between the free-volume as a function of the cavity volume and the total free-volume. The numbers corresponds to the temperature (in units of K) of the simulation samples.

to the formation of cavities of dimension extending along the full length of the simulation box. This gives rise to the artifact that cavities extending on the full length of the box and crossing the box at the boundaries are classified as percolating cavities of infinite dimension. To avoid the consideration of infinite volume cavities we have limited the maximum volume of a cavity to that included in the simulation box. The presence of large cavities has a strong impact on the integral distribution of the free-volume as a function of the cavity volume as shown in Figure 4. The number of large cavities increases at the expenses of the smaller ones as the temperature increases and their dimension is expected to increase by increasing the box size. Large cavities represent a large portion of the free-volume. At 300 K, the formation of large cavities is regular (they are detected in all 500 explored structures) and their typical size is in the range 300–500 Å^3 ($R_{\rm h} = 4.1$–4.9 Å). Actually the integral distribution of Figure 4 shows that at higher temperatures, around 330 K, the total free-volume is localized to a great extent in large cavities. Due to the thermal motion, these cavities will eventually break, their lifetime being too short to allow experimental detection. Clearly, exclusion of their volume from the calculation decreases the mean cavity volume. We conclude therefore that the saturation of the mean cavity volume obtained from PALS measurements (see Fig. 3) is mainly due to dynamic processes rather than to a structural change of the system.

3.4 Free-volume cavity fraction

Another relevant quantity is the free-volume cavity fraction defined as the ratio between the total free-volume and the total volume of the simulation box. In the literature, four semi-empirical models have been proposed [10–14,16,17] for the evaluation of free-volume

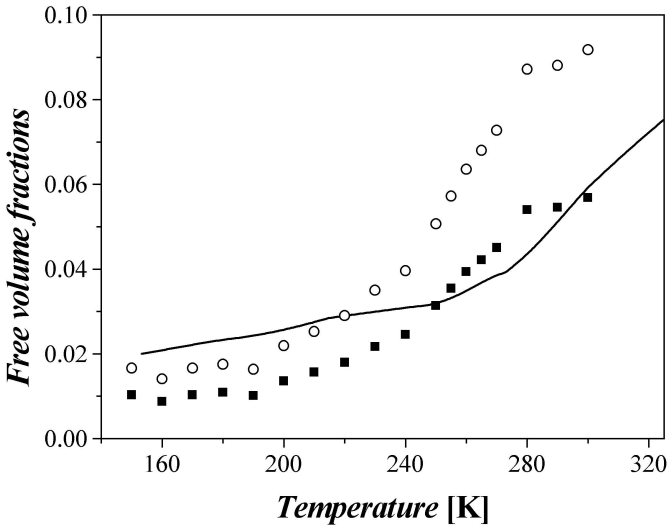

Fig. 5. Free-volume fractions calculated from MD simulations (solid line) and from the simplified semi-empirical models (circles: OSM; squares: TSM). The data from simulations have been obtained considering cavities larger than 30 Å^3.

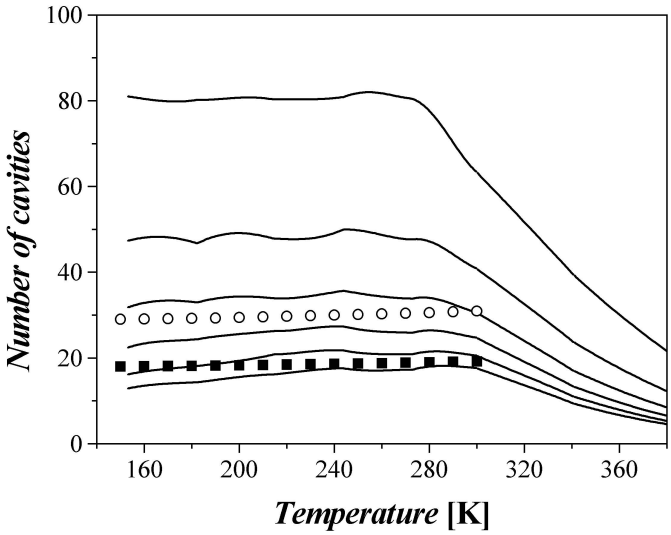

Fig. 6. Number of cavities calculated from MD simulations for different $V_{\rm lim}$ as a function of temperature (solid line; from top to bottom $V_{\rm lim}$ = 5, 10, 15, 20, 25 and 30 Å^3). The number of holes obtained from the simplified models are also reported (circles: OSM; squares: TSM).

hole fraction from PALS data. All of them are based on the thermal expansion of the macroscopic volume and on the microscopic volume hole size obtained from PALS data. Two of these models, called generalized one-state (GOSM [13]) and generalized two-state (GTSM [11,12,14]) models, differ from the others two, the simplified one- (OSM [13,14]) and two-state (TSM [16,17]) models, by the inclusion of the relative PALS intensity in the expression of the free-volume cavity fraction. The two-state models (GTSM and TSM) consider also a temperature dependence of the volume occupied by the molecules. The free-volume hole fractions calculated from the OSM and TSM are plotted in Figure 5 together with the free-volume cavity fractions calculated from the MD simulations for $V_{\rm lim}$ = 30 Å^3. The comparison is given only for two simplified models since at present a precise meaning of the relative intensity in PALS measurements is not available. As found for the mean cavity volumes, the calculated free-volume fractions differ by a factor of about two from the experimental ones in the glass. In the liquid the data from MD simulations agree better with the TSM rather than with the OSM.

Another interesting comparison concerns the number of free-volume cavities. The number of free-volume cavities for various values of $V_{\rm lim}$ is plotted as a function of temperature in Figure 6, together with the results obtained from the OSM and TSM. Figure 6 is equivalent to Figure 2b, with the difference that in the latter all cavities are considered in the calculation, whereas in Figure 6, as pointed out before, cavities of dimension lower than a limiting value are excluded. The figure shows that the number of cavities is now significantly lower than that obtained considering all cavities, indicating the presence of large portions of small cavities in the system. The approximate agreement between the number of cavities calculated from the MD simulations and the number of free-volume holes estimated by the simplified models gives further support to the assumption of the aforementioned models [13,14,16,17] of the temperature-independence of the number of free-volume cavities. The change of slope that in Figure 2b occurs at about 250 K, is now shifted to about 300 K. From this result we can infer that the bending observed in the mean cavity volume at the glass transition (see Fig. 3) can be mainly ascribed to the variation in the total free-volume. This was indeed observed by the calculation of the total free-volume for different $V_{\rm lim}$ (data not shown).

4 Conclusions

We have performed molecular dynamics simulations of glycerol in the liquid and glassy phases to interpret the free-volume data (total free-volume, number of free-volume cavities, mean cavity volume and free-volume cavity fraction) obtained by positron annihilation lifetime spectroscopy (PALS). Glycerol configurations, taken from a series of simulated trajectories at various temperatures, were explored by a virtual probing procedure. Although only a specific system was studied, our analysis furnishes very general and significant information on the interpretation of the experimental free-volume data.

We found that, for glycerol, the calculated mean cavity volumes are much lower than those obtained by PALS experiments. After having tested that the probe radius used in the probing procedure does not affect significantly the calculated free-volume properties, we have demonstrated that agreement between experimental and calculated data can be achieved only assuming the existence of a lower limit for the volume of the cavities detectable by PALS measurements. We find this limiting volume to be

about 25–30 Å^3 in the temperature range 250–275 K. Our results show also that the limiting volume for detectable cavities is temperature-dependent and that it increases by increasing the temperature. The comparison between experimental and calculated mean cavity volume is not feasible above 280 K due to the occurrence of the characteristic PALS temperature called T_{b2}^L. At this temperature a significant bend of the mean cavity volume versus temperature curve has been observed experimentally that is absent in our analysis of the static free-volume. Recent studies ascribed such a behavior to the mean α-relaxation time of glycerol that, at high temperature, is lower than the positronium lifetime. We offer additional support to this empirical finding, showing the possible formation of very large cavities (cavity percolation through the simulation samples) whose lifetime is too short to allow their detection by PALS.

Finally, we compare the free-volume cavity fraction calculated by MD simulations to that estimated from two semi-empirical models, the so-called simplified one- and the two-state models. On the basis of our approximative simulation model we furnish a support to the main assumption of both models that the number of free-volume cavities is temperature-independent, showing that this number is almost constant from the glass up to the room temperature, where cavity percolation starts to appear. This finding is interesting, not only for the aforementioned theoretical implications, but also since it supports the view that in condensed phases a change in the mean cavity volume is due to a variation of the dimension of the single free-volume cavities rather than to cavity break/aggregation phenomena (in the mean statistic sense).

DR thanks the European Laboratory of non-linear Spectroscopy, University of Firenze for providing the Maria Curie Training Fellowship and, together with JB, wish to thank the Vega Agency (Contract No. 2/3026/23) and the APVT grant 51-045302, Slovakia for financial support of this joined research. This work has been also supported by the Italian Ministero dell'Istruzione, dell'Università e della Ricerca (MIUR), and by the European Union (Contract No. HPMT-CT-2000-00123).

References

1. W. Brandt, A. Dupasquier, *Positron Solid State Physics* (North-Holland, Amsterdam, 1983)
2. Y.C. Jean, Characterizing Free Volume and Holes in Polymers by Positron Annihilation Spectroscopy, in *Positron Spectroscopy of Solids,* edited by A. Dupasquier (IOS, Ohmsha, Amsterdam, 1995), pp. 563–580
3. J. Bartoš, Positron Annihilation Spectroscopy of Polymers and Rubbers, in *Encyclopedia of Analytical Chemistry*, edited by R.A. Meyers (Wiley & Sons, Chichester, 2000), pp. 7968–7987
4. Y.C. Jean, Microchem. J. **42**, 72 (1990)
5. S.J. Tao, J. Chem. Phys. **56**, 5499 (1972)
6. M. Eldrup, D. Lightbody, J.N. Sherwood, Chem. Phys. **63**, 51 (1981)
7. H. Nakanishi, S.J. Wang, Y.C. Jean, in *Positron Annihilation Studies of Fluids*, edited by S.C. Sharma (World Science, Singapore, 1988)
8. T. Mukherjee, S.K. Das, B.N. Ganguly, B. Dutta-Roy, Phys. Rev. B **57**, 13363 (1998)
9. A.J. Kovacs, Fortschr. Hochpolym.-Forsch. **3**, 394 (1964)
10. Y. Kobayashi, W. Zheng, E.F. Meyer, J.D. McGervey, A.M. Jamieson, R. Simha, Macromolecules **22**, 2302 (1989)
11. Y.Y. Wang, H. Nakanishi, Y.C. Jean, T.C. Sandreczki, J. Polym. Sci. B **28**, 1431 (1990)
12. H. Nakanishi, Y.C. Jean, E.G. Smith, T.C. Sandreczki, J. Polym. Sci. B **27**, 1419 (1989)
13. J. Bartoš, J. Krištiak, J. Phys. Chem. B **104**, 5666 (2000)
14. J. Bartoš, O. Šauša, J. Krištiak, *Non-linear Dielectric Phenomena in Complex Liquids*, ARW NATO Series (Kluwer Acad. Publ., Dordrecht, The Netherlands, 2004), p. 289
15. M. Welander, F.H.K. Maurer, Mater. Sci. Forum **105-110**, 1811 (1992)
16. P. Bandžuch, J. Krištiak, O. Šauša, J. Zrubcová, Phys. Rev. B **61**, 8784 (2000).
17. G. Consolati, M. Levi, L. Messa, G. Tieghi, Europhys. Lett. **53**, 497 (2001)
18. A.J. Batschinski, Z. Phys. Chem. **84**, 643 (1913)
19. T.G. Fox, P.J. Flory, J. Appl. Phys. **21**, 581 (1950)
20. A.K. Doolittle, J. Appl. Phys. **22**, 1031 (1951)
21. D. Turnbull, M.H. Cohen, J. Chem. Phys. **34**, 120 (1961)
22. G.S. Grest, M.H. Cohen, Adv. Chem. Phys. **48**, 455 (1981)
23. E.G. Kim, S. Misra, W.L. Mattice, Macromolecules **26**, 3424 (1993)
24. D. Rigby, R.J. Roe, Macromolecules **23**, 5312 (1990)
25. S. Lee, W.L. Mattice, Comput. Theor. Polym. S. **9**, 57 (1999)
26. R.M. Dammert, S.L. Maunu, F.H.J. Maurer, I.M. Neelov, S. Niemelä, F. Sundholm, C. Wästlund, Macromolecules **32**, 1930 (1999)
27. V.M. Shah, S.A. Stern, P.J. Ludovice, Macromolecules **22**, 4660 (1989)
28. M.L. Connolly, J. Appl. Cryst. **16**, 548 (1983)
29. T.J. Richmond, J. Mol. Biol. **178**, 63 (1984)
30. M.L. Connolly, J. Am. Chem. Soc. **107**, 1118 (1985)
31. S. Arizzi, P.H. Mott, U.W. Suter, J. Polym. Sci. B **30**, 415 (1992)
32. J.L. Finney, Proc. R. Soc. London A **319**, 479 (1970)
33. W. Brostow, J.P. Dussault, B.L. Fox, J. Comput. Phys. **29**, 81 (1978)
34. M. Tanemura, T. Ogawa, N. Ogita, J. Comput. Phys. **51**, 191 (1983)
35. N.N. Medvedev, J. Comput. Phys. **67**, 223 (1986)
36. S. Sastry, D.S. Corti, P.G. Debenedetti, F.H. Stillinger, Phys. Rev. E **56**, 5524 (1997)
37. J. Bartos, J. Urban, P. Mach, J. Kristiak, Mater. Sci. Forum **363-365**, 294 (2001)
38. M.P. Allen, D.J. Tildesley, *Computer Simulation of Liquids* (Clarendon Press, Oxford, 1987)
39. D. Frenkel, B. Smit, *Understanding Molecular Simulation* (Academic Press, San Diego, 1996)
40. R. Chelli, P. Procacci, G. Cardini, R.G. Della Valle, S. Califano, Phys. Chem. Chem. Phys. **1**, 871 (1999)
41. R. Chelli, P. Procacci, G. Cardini, S. Califano, Phys. Chem. Chem. Phys. **1**, 879 (1999)

42. J. Bartos, O. Sausa, P. Bandzuch, J. Zrubcova, J. Kristiak, J. Non-Cryst. Solids **307**, 417 (2002)
43. J. Bartos, O. Sausa, J. Kristiak, T. Blochowicz, E. Rössler, J. Phys.-Cond. Matter **13**, 11473 (2001)
44. K.L. Ngai, P. Lunkenheimer, C. Leon, U. Schneider, R. Brand, A. Loidl, J. Chem. Phys. **115**, 1405 (2001)
45. J. Wuttke, J. Hernandez, G. Li, G. Coddens, H.Z. Cummins, F. Fujara, W. Petry, H. Sillescu, Phys. Rev. Lett. **72**, 3052 (1994)
46. T. Darden, D. York, L. Pedersen, J. Chem. Phys. **98**, 10089 (1993)
47. P. Procacci, T.A. Darden, E. Paci, M. Marchi, J. Comput. Chem. **18**, 1848 (1997)
48. P. Procacci, T. Darden, M. Marchi, J. Phys. Chem. **100**, 10464 (1996)
49. S. Sastry, T.M. Truskett, P.G. Debenedetti, S. Torquato, F.H. Stillinger, Mol. Phys. **95**, 289 (1998)
50. A.K. Schultz, Kolloid Z. **138**, 75 (1954)
51. T. Blochowicz, A. Kudlik, S. Benkhof, J. Senker, E. Rössler, G. Hinze, J. Chem. Phys. **110**, 12011 (1999)
52. C.M. McCullagh, Z. Yu, A.M. Jamieson, J. Blackwell, J.D. McGervey, Macromolecules **28**, 6100 (1995)
53. A. Szymoszek, A. Koll, Chem. Phys. Lett. **373**, 591 (2003)
54. Z. Yu, Ph.D. thesis, Case Western Reserve University (1995)